The electronic structure of alkali metals: experiment and theory



1993 J. Phys.: Condens. Matter 5 8703

(http://iopscience.iop.org/0953-8984/5/46/009)

J. Phys.: Condens. Matter 5 (1993) 8703–8724. Printed in the UK

# The electronic structure of alkali metals: experiment and theory

A A Manuel†, L Oberli†¶, A K Singh†*, T Jarlborg†, M Peter†, P E Mijnarends‡, L P L M Rabou§, T Hyodo‖+ and A T Stewart‖

† Département de Physique, Université de Genève, 1211 Genève 4, Switzerland
‡ Interfaculty Reactor Institute, Delft University of Technology, Mekelweg 15, 2629 JB Delft, The Netherlands
§ Netherlands Energy Research Foundation (ECN), 1755 ZG Petten, The Netherlands
‖ Department of Physics, Queen's University, Kingston, Ontario K7L 3N6, Canada

Received 24 June 1993

**Abstract.** The high-momentum components of the electron and positron Bloch waves in the three alkali metals Li, Na, and K have been studied by comparing calculations employing the linear muffin tin orbital method and the independent particle model with accurate measurements of the two-dimensional angular correlation of annihilation radiation. It is found that such an analysis provides a sensitive test of electronic structure, and that electron–positron correlation effects do not distort the high-momentum components in this example in any significant way. It is shown that thermal effects due to Debye–Waller damping are important.

## 1. Introduction

Positrons shot into metals thermalize and then annihilate, mostly with the conduction electrons. The usual annihilation process yields two gamma rays—each with energy of $mc^2 \sim 0.511$ MeV—which are at 180° to each other in the centre of mass system. In the laboratory, the slight departure from 180° yields directly the momentum of the electron–positron pair, which, since the positron is thermalized, is the momentum of the electron annihilated. The angular correlation of these annihilation photons has become a unique and useful method for studying several features of solids ranging from simple metals to complex compounds and alloys [1]. The first feature is of course the Fermi surface. Positron annihilation work can yield dimensions of the Fermi surface with a precision better than 1% in favourable cases; not as good as the best de Haas–van Alphen area measurements but easily comparable with most other techniques. Not requiring a long free path of the electrons, the positron technique can also observe the Fermi surface of alloys.

Secondly the technique can also provide information about the lattice modulation of the wave function. As first pointed out by DeBenedetti *et al* [2], these high-momentum components (HMCs) of the Bloch states can be observed directly.

Finally the technique can measure some features of the many-body interactions of the electron gas. Ferrell [3] noted that the negative polarization cloud formed around the

¶ Present address: CERN, CH-1211 Geneva 23, Switzerland.

* Present address: HB Technological Institute, Kanpur 208 002, India.

\+ Present address: Institute of Physics, College of Arts and Sciences, University of Tokyo, Komaba 3-8-1, Meguro-ku, Tokyo 153, Japan.

0953-8984/93/468703+22$07.50  

positron has a central density many times that of the average of the conduction electrons. The enhanced density has a momentum distribution that is also somewhat different from that of the valence electrons in the metal.

The alkali metals are simple enough that they provide good tests for the examination of these features by modern good resolution angular correlation experiments and modern band structure calculational methods. Considerable information on all the features mentioned above has been drawn from the data already obtained from the conventional 'long-slit' apparatus for measuring one component of momentum. In this study we present band structure calculations and two-dimensional momentum measurements for the metals lithium, sodium, and potassium, and the temperature dependence of some of these data.

The alkali metals are particularly useful for testing calculations of the momentum density $\rho(\boldsymbol{p})$ because of their relatively simple electronic structure. Calculations of the two-photon momentum density $\rho^{2\gamma}(\boldsymbol{p})$ of the annihilation photons are commonly performed in the independent particle model, i.e., the electron and positron wave functions are determined using an effective one-particle potential. In general this approximation yields satisfactory results. However, careful analyses [4–8] of experimental data have established that a many-body enhancement factor of the type proposed by Kahana and Carbotte [9–11] improves the agreement between experiment and theory in the first Brillouin zone. Hence the question arises of what way the Umklapp components in the higher Brillouin zones are affected by many-body interactions. Hede and Carbotte [12] were the first to approach this problem theoretically. They concluded that the enhancement of the HMCs was similar in value and in momentum dependence to that of the central part of the distribution. Fujiwara *et al* [13, 14] studied a two-band nearly free electron model and found that either enhancement or 'dehancement' (i.e. diminution) of the higher components could occur, depending on the relative importance of the intraband and interband transitions. In the alkali metals with their half filled bands, intraband transitions are possible and dominate the enhancement process, leading to an enhancement in higher zones similar to that of the central zone. A different conclusion was reached by Sormann and Puff [15] who found considerable dehancement in higher zones.

Systematic and detailed experimental investigations of enhancement in higher zones are scarce. The first two-dimensional data for Al [16] showed that the intensity of conduction band Umklapp components agreed well with orthogonalized plane wave predictions, implying that the higher momentum components are enhanced by a similar amount to the lower-momentum part of the distribution. Similar conclusions were reached in the case of Cu [17], but a recent study of Ni [6] suggests that the situation in transition metals may be more complicated. These complications in the enhancement factor may be caused by the nature of the wave function itself as shown by Fujiwara *et al* [13, 14].

The core contribution in the momentum distribution of photons from positrons annihilating in alkali metals is not easily understood. As most calculations of the core distributions are wider than those measured, experimentalists sometimes prefer to use momentum distributions similar to those observed in solid He, Ne, and Ar corresponding to Li, Na, and K [7, 8]. The reason for the discrepancy remains unresolved. It is sometimes suggested that electron–positron correlation effects are responsible and perhaps the inevitable oxidation may also contribute. We suggest that the Debye–Waller factor may account for part of the problem. To date it has not been included in these studies of alkali metals despite the small masses involved and the high (reduced) temperature of some of the experimental work. A modified approach to applying the Debye–Waller factor is proposed.

In section 2 we describe the theoretical background needed to discuss our results, with a special mention of temperature effects for which we propose a modified description.

Section 3 is devoted to band structure calculations performed using the linear muffin tin orbital (LMTO) method. Section 4 contains the description of the experiment and a presentation of the results. In section 5 we discuss the calculated and observed HMCs of the wave functions in terms of the atomic orbital character of these functions. A few preliminary results of this part of the work have been published [7, 18], but a complete account of the entire work is needed and is presented in this paper. Finally we discuss how these results change with temperature. Our conclusions are summarized in section 6.

## 2. Theory

### *2.1. Momentum distribution of annihilation photons*

The two-dimensional angular correlation of positron annihilation radiation is given by

$$N(p_x, p_y) = \int \rho(\boldsymbol{p})\,\mathrm{d}p_z \tag{1}$$

where $\rho(\boldsymbol{p})$ is the two-photon momentum distribution† given in the independent particle approximation by

$$\rho(\boldsymbol{p}) = \sum_{\mathrm{occ}} \left| \int \exp(\mathrm{i}\boldsymbol{p}\cdot\boldsymbol{r})\Psi_{k,j}(\boldsymbol{r})\Psi_{+}(\boldsymbol{r})\,\mathrm{d}\boldsymbol{r} \right|^2 \tag{2}$$

and where $\Psi_{k,j}(\boldsymbol{r})$ and $\Psi_{+}(\boldsymbol{r})$ are the electron and (thermalized) positron wave functions. The sum is over all the occupied $(\boldsymbol{k}, j)$ electronic states where $\boldsymbol{k}$ is the wave vector and $j$ is the band index. In the (LMTO) representation [19–21] the wave functions are taken to be

$$\Psi(\boldsymbol{r}) = \sum_{lm} i^l a_{lm}^{k,j} Y_{lm}(\boldsymbol{r}) R_l(E_{k,j}, \boldsymbol{r}) \tag{3}$$

and

$$\Psi_{+}(\boldsymbol{r}) = R_0^{+}(E^{+}, \boldsymbol{r}) \tag{4}$$

where the $a_{lm}^{k,j}$ are coefficients of eigenvectors, $Y_{lm}$ the spherical harmonic functions, $R_l$ the $l$-state radial electron wave function and $R_0^{+}$ the $l = 0$ wave function of the positron in its lowest state. It should be noted that the annihilation photon momentum distribution differs from that of the electrons by the positron wave function which appears in equation (2).

The photon momentum distribution defined in equation (2) may be expressed in a plane wave expansion as

$$\rho(\boldsymbol{p}) = \text{constant} \times \sum_{k,j} |C_{k,j}(\boldsymbol{G})|^2 \delta(\boldsymbol{p} - \boldsymbol{k} - \boldsymbol{G}) \tag{5}$$

where the $C_{k,j}(\boldsymbol{G})$ are the Fourier coefficients in the plane wave expansion of the product of the electron and positron wave functions:

$$\Psi_{k,j}\Psi_{+} = \sum_{\boldsymbol{G}} C_{k,j}(\boldsymbol{G}) \exp[\mathrm{i}(\boldsymbol{k} + \boldsymbol{G})\cdot\boldsymbol{r}]. \tag{6}$$

† From here onward we drop the superscript $2\gamma$.

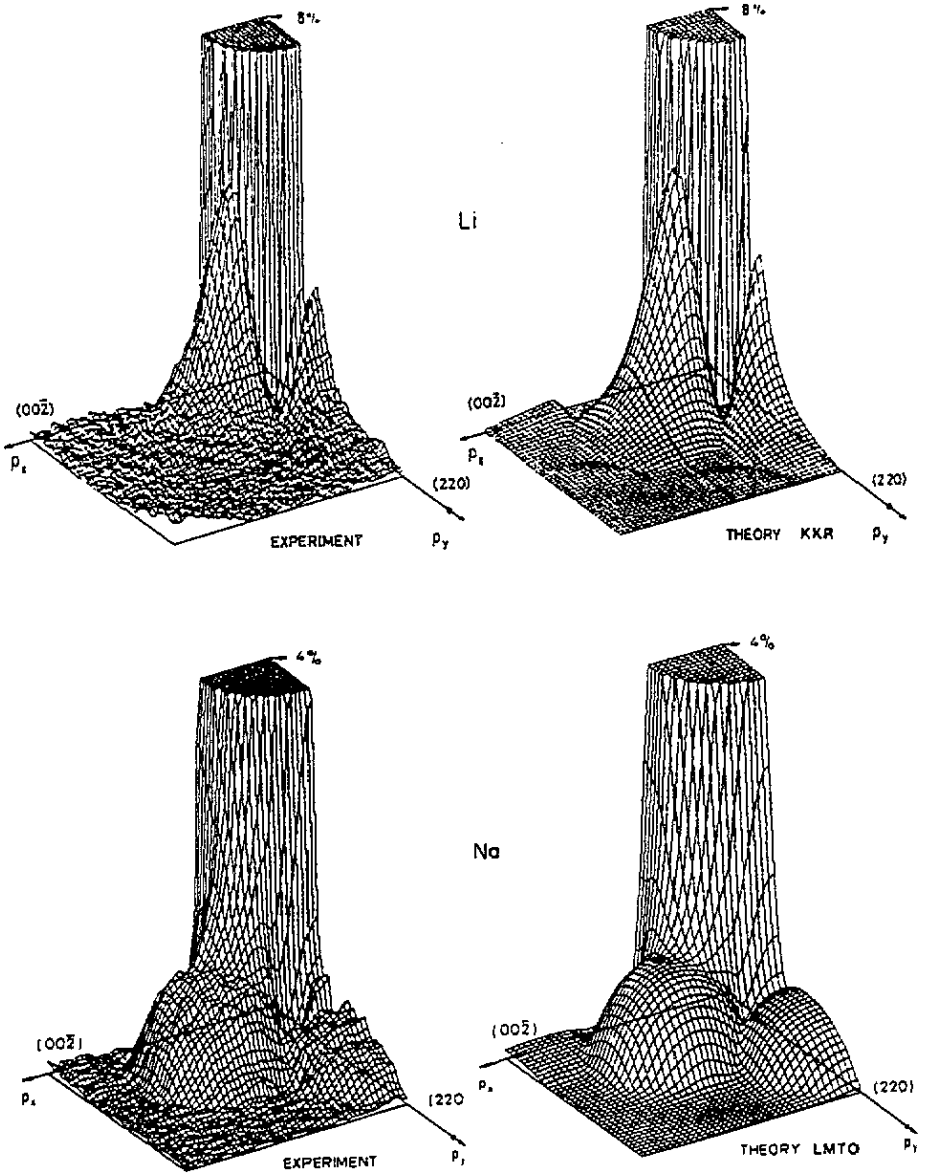


**Figure 1.** Measured and calculated momentum distributions of photons from positrons annihilating in Li, Na, and K. The vertical scale has been expanded to display the HMCs of the electron–positron wave function product. The central portion has been cut-off at 4% or 8% of the height at the origin.

In order to obtain the plane wave coefficients $C_{k,j}(G)$ from the LMTO function a correction is needed to account for the overlapping spheres [22]. Thus we have

$$C_{k,j}(G) = \sum_{G'} M^{-1}_{G,G'} X^{k,j}_{G'} \tag{7}$$

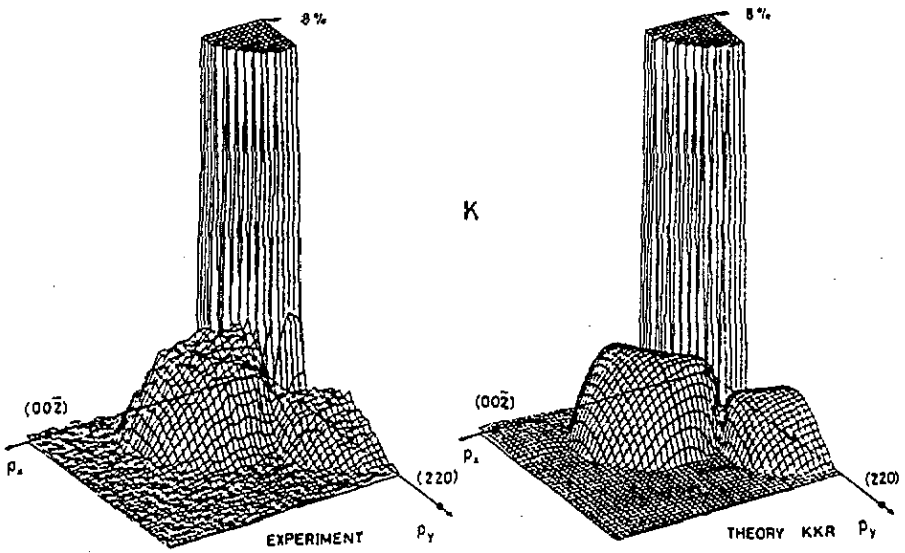


**Figure 1.** (Continued)

where

$$M_{G,G'} = \int_{\text{sphere}} \exp[\mathrm{i}(\boldsymbol{G}-\boldsymbol{G}')\cdot\boldsymbol{r}]\,\mathrm{d}\boldsymbol{r} = \frac{4\pi}{3}R_{\text{WS}}^3\frac{3j_1(|\boldsymbol{G}-\boldsymbol{G}'|R_{\text{WS}})}{|\boldsymbol{G}-\boldsymbol{G}'|R_{\text{WS}}} \tag{8}$$

$$X_G^{k,j} = 4\pi\sum_{lm} a_{lm}^{k,j}Y_{lm}(\boldsymbol{k}+\boldsymbol{G})\int_0^{R_{\text{WS}}} R_l(E_{k,j},r)R_0^+(r)j_l(|\boldsymbol{k}+\boldsymbol{G}'|r)r^2\,\mathrm{d}r. \tag{9}$$

Here, radial integrations are performed over the Wigner–Seitz radius $R_{\text{WS}}$.

It is now possible to write the following expression for $\rho(\boldsymbol{p})$:

$$\rho(\boldsymbol{p}) = \text{constant}\times\sum_{k,j}\sum_{G}|B_{lm}(\boldsymbol{p})|^2 \qquad \boldsymbol{p}=\boldsymbol{k}+\boldsymbol{G} \tag{10}$$

where

$$B_{lm}(\boldsymbol{p}) = 4\pi\sum_{G'}M_{G,G'}^{-1}a_{lm}^{k,j}Y_{lm}(\boldsymbol{k}+\boldsymbol{G})\int_0^{R_{\text{WS}}} R_l(E_{k,j},r)R_0^+(r)j_l(|\boldsymbol{k}+\boldsymbol{G}'|r)r^2\,\mathrm{d}r. \tag{11}$$

These equations are useful to understand the $l$-character of the various parts of the HMCs of the wave functions.

### *2.2. Electron–positron correlation effects*

The interactions between the positron and all the electrons are known to modify appreciably the independent particle picture for metals. The lifetime is an order of magnitude shorter, and

the momentum distribution of photons from positrons annihilating with conduction electrons in alkali metals differs slightly from that expected from free electron theory [4, 23–28]. We will use the simple description first given by Kahana and Carbotte [9–11] some thirty years ago

$$\rho(\boldsymbol{p}) = \epsilon(|\boldsymbol{p}|)\rho^{\mathrm{IPM}}(\boldsymbol{p}) \tag{12}$$

where $\epsilon(p)$ is called the enhancement factor and has the approximate form

$$\epsilon(p) = a + b(p/p_{\mathrm{F}})^2 + c(p/p_{\mathrm{F}})^4. \tag{13}$$

The careful analysis by Hyodo *et al* [8] shows that this description fits the data better than more recent calculations.

### *2.3. Thermal effects and the Debye–Waller factor*

There are several kinds of thermal effects that change the characteristic properties of positron annihilation [29]. We shall discuss here mainly two: thermal expansion of the crystal lattice and thermal vibrations of the ions about their equilibrium positions. The former, the increase in lattice size with temperature, can be included by performing the calculations for a different lattice constant appropriate to each temperature. Alternatively, if the band structure does not change significantly with lattice expansion a simple renormalization may account for this effect.

It is much more difficult to include the effect of thermal vibrations of ions because both positrons and electrons are affected. In contrast with x-ray scattering in which the electrons doing most of the scattering are closely associated with the nucleus, positrons are mostly in interstitial regions and annihilate with electrons least attached to the nuclei. Furthermore, the wavelength of the positron probe is about one order of magnitude larger than the lattice constant while the x-ray wavelength is comparable to or smaller than the interatomic distance. Because of these facts the effect of thermal vibrations on positron annihilation should be more carefully analysed. Brandt *et al* [30] were the first to investigate these effects. According to their ideas thermal vibrations modify the annihilation photon momentum distribution in the same way as in x-ray measurements. This is expressed as

$$\rho(\boldsymbol{p}) = \sum_{k,j} |C_{k,j}(\boldsymbol{G})|^2 \exp[-2W(\boldsymbol{G}, T)]\delta(\boldsymbol{p} - \boldsymbol{k} - \boldsymbol{G}) \tag{14}$$

where $C_{k,j}(\boldsymbol{G})$ are the plane wave coefficients for the frozen lattice described in the previous section. The factor $\exp[-2W(\boldsymbol{G}, T)]$ is known as the Debye–Waller factor. It reduces the contribution of the zone corresponding to the reciprocal lattice vector $\boldsymbol{G}$. For cubic crystals the function $W$ can be expressed as [31]

$$W(\boldsymbol{G}, T) = \tfrac{3}{2}\big(\hbar^2 G^2/Mk_{\mathrm{B}}\theta_{\mathrm{D}}\big)\big[\tfrac{1}{4} + \big(T/\theta_{\mathrm{D}}\big)\phi\big(\theta_{\mathrm{D}}/T\big)\big] \tag{15}$$

where $M$ is the atomic mass of the ion, $\theta_{\mathrm{D}}$ the Debye temperature, $k_{\mathrm{B}}$ the Boltzmann constant and $\phi(x)$ the Debye function. When described by equation (15) the Debye–Waller factor is constant in each zone. For filled bands this leads to a discontinuity at the zone boundary. To avoid this problem we propose to use a $\boldsymbol{p}$-dependent function $W(\boldsymbol{p}, T)$, which is a continuous function defined everywhere in reciprocal space. We can write $W(\boldsymbol{p}, T)$ as follows:

$$W(\boldsymbol{p}, T) = \tfrac{3}{2}\big(2\pi/a_0\big)^2\Big(\hbar^2/Mk_{\mathrm{B}}\theta_{\mathrm{D}}\Big)\big[\tfrac{1}{4} + \big(T/\theta_{\mathrm{D}}\big)\phi\big(\theta_{\mathrm{D}}/T\big)\big]q^2 \tag{16}$$

with $\boldsymbol{p} = \boldsymbol{G} + \boldsymbol{k} = (2\pi/a_0)\boldsymbol{q}$ and $a_0$ the lattice constant. We shall use both equation (15) and equation (16) to analyse the data and shall find that equation (16) gives a somewhat better agreement with experiment.

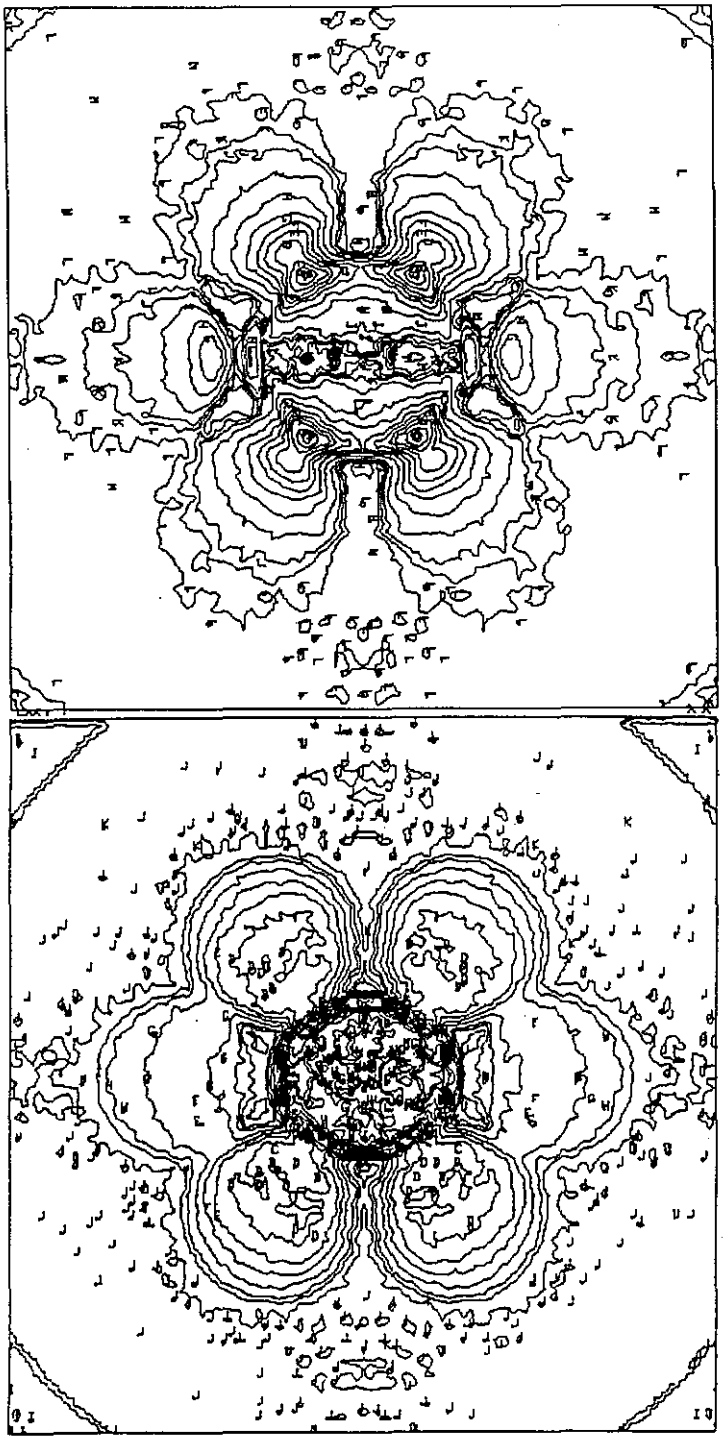

**Figure 2.** From the observational data shown in figure 1: contours of projected momentum density for the higher momentum components of the distribution for Li (above) and K (below). The contours in the first zone result from a subtraction process and have no significance.

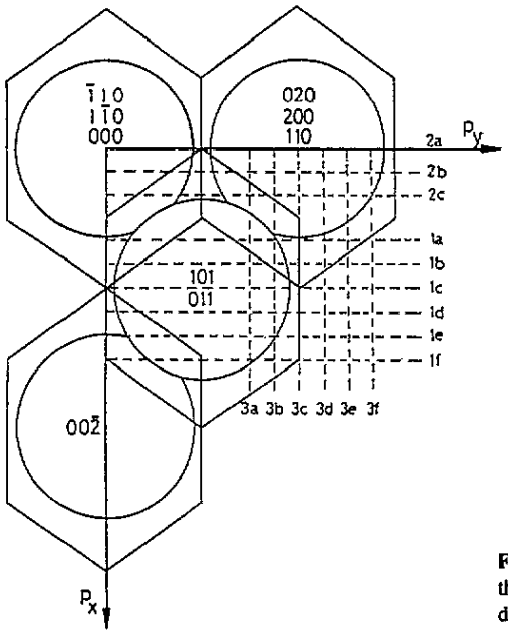


**Figure 3.** Projection of extended Brillouin zones in the (110) plane showing the location of profiles to be displayed in figures 4, 5, and 6.

## 3. Calculations

The band structures have been calculated self-consistently using the LMTO method [19, 20]. The valence basis set was semirelativistic and included s, p, d, and f states. The core levels were fully relativistic and have been included in the iteration to self-consistency. In the case of K a completely non-relativistic calculation has also been performed but no noticeable difference was found compared to the semi-relativistic calculation. The d states play an important role in the HMCs of the wave functions in K despite the largely free electron like properties of this metal. A non-optimal choice of $E_d$ (the energy at which the linearized d orbital is calculated) more than 0.5 Ryd higher than $E_F$ leads to noticeable changes in the results for the HMCs. In the results presented here $E_d$ lies approximately 0.2 Ryd above $E_F$ in all cases. In these calculations the errors due to linearization are very small. Table 1 gives the partial $l$-character of the valence electron distribution in the different metals.

**Table 1.** Angular momentum decomposition of the valence electron charge obtained from the LMTO calculations.

| | Li | Na | K |
|---|---|---|---|
| s | 0.509 | 0.612 | 0.604 |
| p | 0.457 | 0.341 | 0.348 |
| d | 0.031 | 0.044 | 0.046 |
| f | 0.003 | 0.003 | 0.002 |

The final band structures were calculated on a fine mesh of 3311 $k$ points in the irreducible Brillouin zone, thereby enabling an accurate interpolation of the higher momentum component results. The electron–positron matrix element was calculated using the electron and positron LMTO wave functions in the independent particle model (IPM). Corrections for the overlap of the Wigner–Seitz zones were included. The effect of

temperature has been taken into account by inclusion of the Debye–Waller factor. Table 2 shows that these temperature effects vary substantially in the alkali metals and cannot be neglected. Even at 0 K there is a sizable reduction of the HMCs due to zero point motion. Finally, to examine the effect of thermal expansion, self-consistent band structure and annihilation momentum distributions were calculated for two lattice parameters (9.882 and 9.916 au) for K.

**Table 2.** The Debye temperature $\theta_D$ and the Debye–Waller factor $\exp(-2W)$ (equation (15)) for the first two HMCs at 0 and 75 K [48].

| | $\theta_D$ (K) | $(a/2\pi)G$ | $\exp(-2W)$ 0 K | $\exp(-2W)$ 75 K |
|---|---|---|---|---|
| Li | 363 | 110 | 0.91 | 0.88 |
| | | 200 | 0.83 | 0.78 |
| Na | 150 | 110 | 0.95 | 0.90 |
| | | 200 | 0.91 | 0.81 |
| K | 100 | 110 | 0.97 | 0.92 |
| | | 200 | 0.95 | 0.84 |

In another set of calculations the Korringa–Kohn–Rostoker (KKR) method [7, 18, 32] was used to calculate the band structure and the photon momentum distribution.

## 4. Experiment and data

The measurements were performed using a high-resolution two dimensional angular correlation apparatus [33]. The distance from specimen to detector was 10.5 m and the positron source was 50 mCi of $^{22}$Na. The growing of the single crystals has been described for Li and Na in [34] and [35] and for K in [8]. The data were obtained at 98 K for Li, at 60 K for Na, and at 4.2 K for K. The temperatures for Li and Na were chosen to avoid the martinsitic phase transitions in these metals. The measurements for K were repeated at 75 K to verify that the reduction of the HMCs is well described by the Debye–Waller factor.

The instrumental resolution function was determined with care by recording the positronium peak in quartz on a very fine mesh (0.05 mrad). We found that it can be described to a good approximation as the sum of a Gaussian function and a Lorentzian function. From this fitting a resolution function was obtained that reproduced accurately the smearing of the Fermi cut off. The parameters describing this resolution function are given in table 3. It should be noted that a tail in the positronium peak was also observed by Fujiwara [36].

**Table 3.** Experimental parameters. The total resolution function $R$ is given by $R = xg+(1-x)L$, where $g$ and $L$ represent its Gaussian and Lorentzian components, and $x$ and $1-x$ denote the respective weights.

| | Li | Na | K | K |
|---|---|---|---|---|
| Temperature (K) | $98 \pm 2$ | $60 \pm 5$ | 4.2 | $75 \pm 2$ |
| Total number of counts | $2.2 \times 10^7$ | $7.6 \times 10^7$ | $6.7 \times 10^7$ | $5.4 \times 10^7$ |
| FWHM of Gaussian (mrad) | $0.42 \times 0.42$ | $0.35 \times 0.33$ | $0.23 \times 0.20$ | $0.38 \times 0.37$ |
| FWHM of Lorentzian (mrad) | $0.20 \times 0.20$ | $0.20 \times 0.20$ | $0.20 \times 0.20$ | $0.20 \times 0.20$ |
| $x$ | 0.60 | 0.65 | 0.75 | 0.65 |

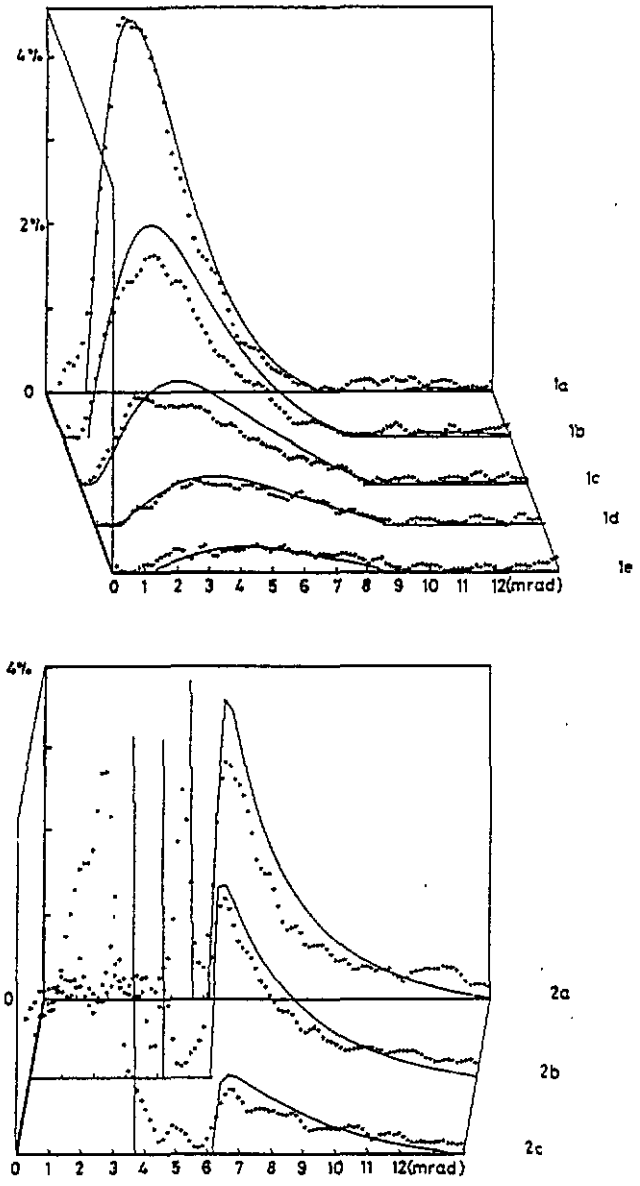


**Figure 4.** Measured and calculated momentum intensities along the profile lines shown in figure 3. The low momentum points in profiles 2a, 2b, and 2c are the residue of the central zone subtraction and have no significance. Li at 98 K; LMTO calculation.

Positrons annihilate with the conduction electrons and with the electrons of the ion cores, $Li^+$, $Na^+$, and $K^+$. The purpose of this paper is to examine the conduction electrons

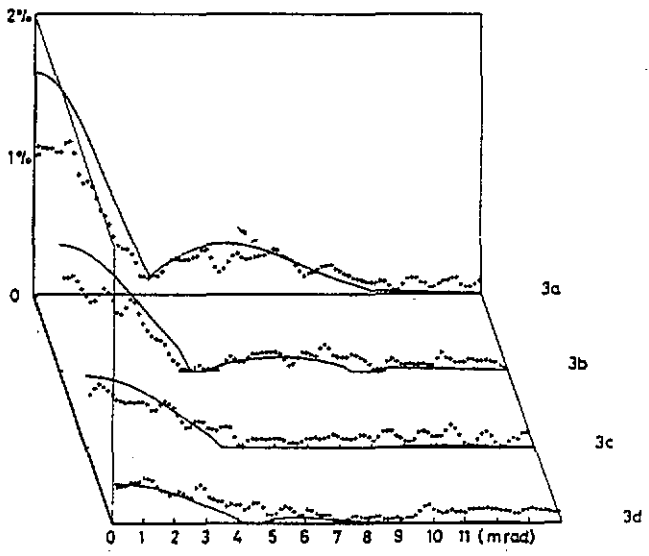


**Figure 4.** (Continued)

and thus it is necessary to subtract the core contribution from the total data recorded. We have first tried to fit the data with the calculated core contribution and then with momentum distributions constructed from angular correlation measurements in the rare gases [37]. Neither procedure gave a very satisfactory result. However, in the case of one electron metals another procedure is possible. In certain orientations of the reciprocal lattice the various Fermi spheres of the higher momentum parts of the wave function can be precisely superimposed leaving clear unobstructed 'views' through reciprocal space. An example of this is shown in figure 3, which we shall discuss later. In these unobstructed regions the momentum distribution has no contribution from the conduction electrons and the data are thus a direct measure of the core intensity at that point. These intensities can be fitted to a smooth function, assumed to be rotationally invariant and subtracted numerically. This procedure should separate the HMCs with a precision of 0.5% of the peak intensity without affecting their shape significantly. The experimental results with the core part thus subtracted are shown in figure 1 in isometric projection. To display the HMCs of this measured momentum distribution, the vertical scale has been expanded and the projection of the nearly free electron Fermi surface cut off at 4% and 8% of the central peak height. In addition a theoretical calculation of the momentum distribution is displayed using the same scale.

In figure 2 the same data are shown plotted as intensity contours for Li and K. Note that these are original data not even folded about the symmetry axes.

## 5. Results and discussion

The alkali metals are the most free electron like of all metals. The Fermi surfaces are nearly spherical; in K the Fermi wave vector $k_F$ has a length variation of less than 0.25% [38],

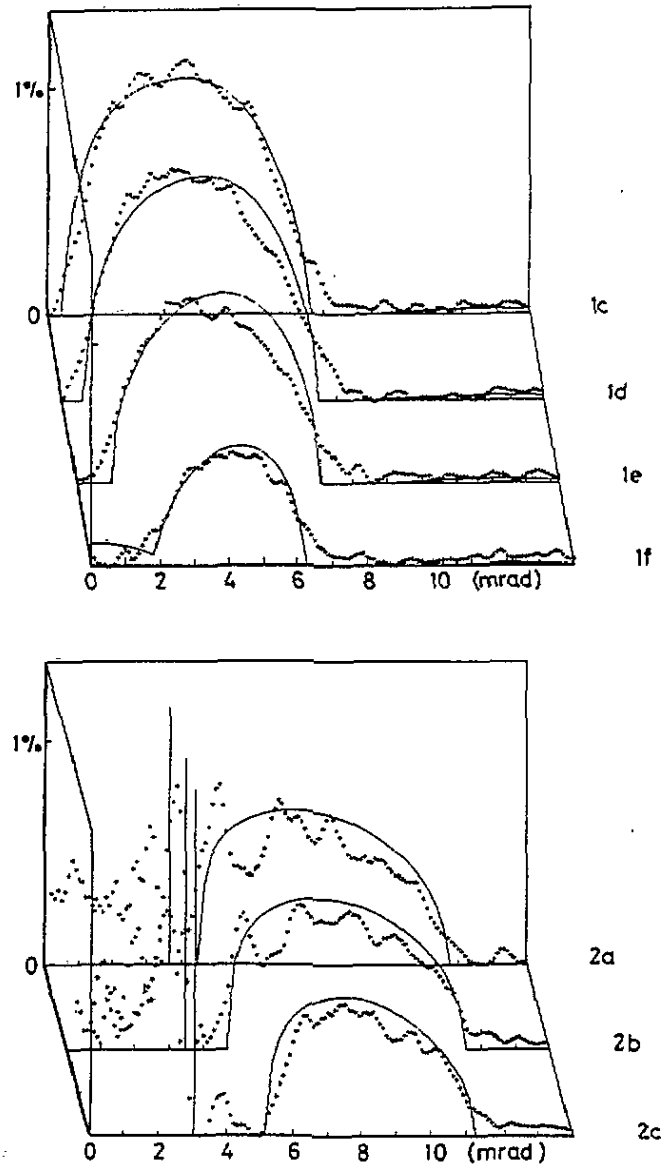


**Figure 5.** As in figure 4. Na at 60 K; LMTO calculation.

and for Na the variation is less than 0.17% [38]. For Li these data yield the best dimensions of the Fermi surface which show 2.8± 0.6% variation having twelve 'bumps' in the [110] directions [35]. The small differences that exist between these metals can best be seen in their electron wave functions. Since the effect of the crystal lattice on these nearly free electrons is small it must be looked for not in the slight diminution of the principal plane wave itself, but rather in the creation in the wave function of harmonics of the periodic

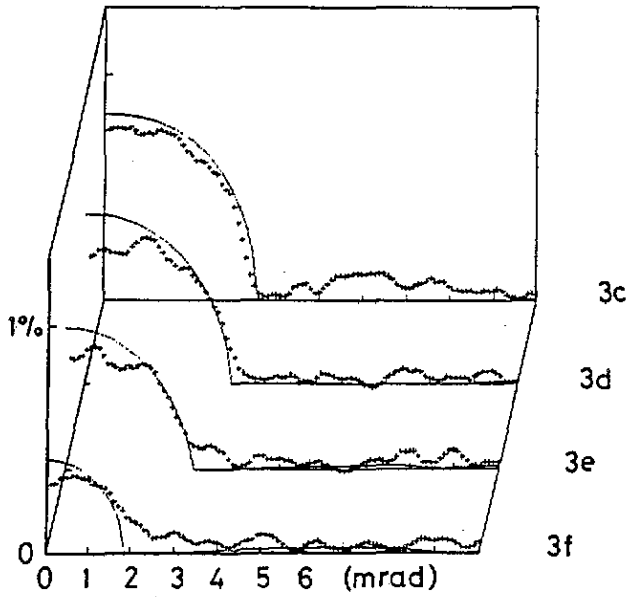


**Figure 5.** (Continued)

crystal potential. These higher harmonics are observed in the momentum distributions in Li, Na, and K.

In the following, section 5.1 contains a discussion of the HMCs of the wave functions, comparing experimental and theoretical results. Section 5.2 presents a discussion of the effects of thermal motion of the ions on the momentum distributions. Section 5.3 contains a summary of other deductions from this experiment.

### *5.1. Higher-momentum components in Li, Na, and K*

The experimental data shown in figures 1 and 2 are presented in this section as intensity profiles taken along the many dashed lines of figure 3, and compared directly with the appropriate calculated results for $\rho(p)$ integrated along a line at right angles to this (110) plane, i.e. the integral equation (1). These measurements and calculations are presented in figures 4, 5, and 6 for Li, Na, and K respectively. The calculated results were obtained using the LMTO band structure method. The calculations obtained in this way are normalized to the peak intensity of the experimental data after inclusion of the Debye–Waller factor (see below), and subtraction of the core electron contribution from the data as described in section 4. It can be seen immediately that the HMCs of these three metals have different shapes and intensities and, remarkably, that the theory is able to provide a good understanding of the differences from one metal to another. A full discussion of this will follow after some comments on the effect of electron–positron correlations.

The first and remarkable observation is that the independent particle model yields HMCs of the wave functions very much like the experimental data. Various models of the electron potential give results that are slightly different one from another, but all are of the correct general shape and all are within about 15% of the measured intensities. This conclusion

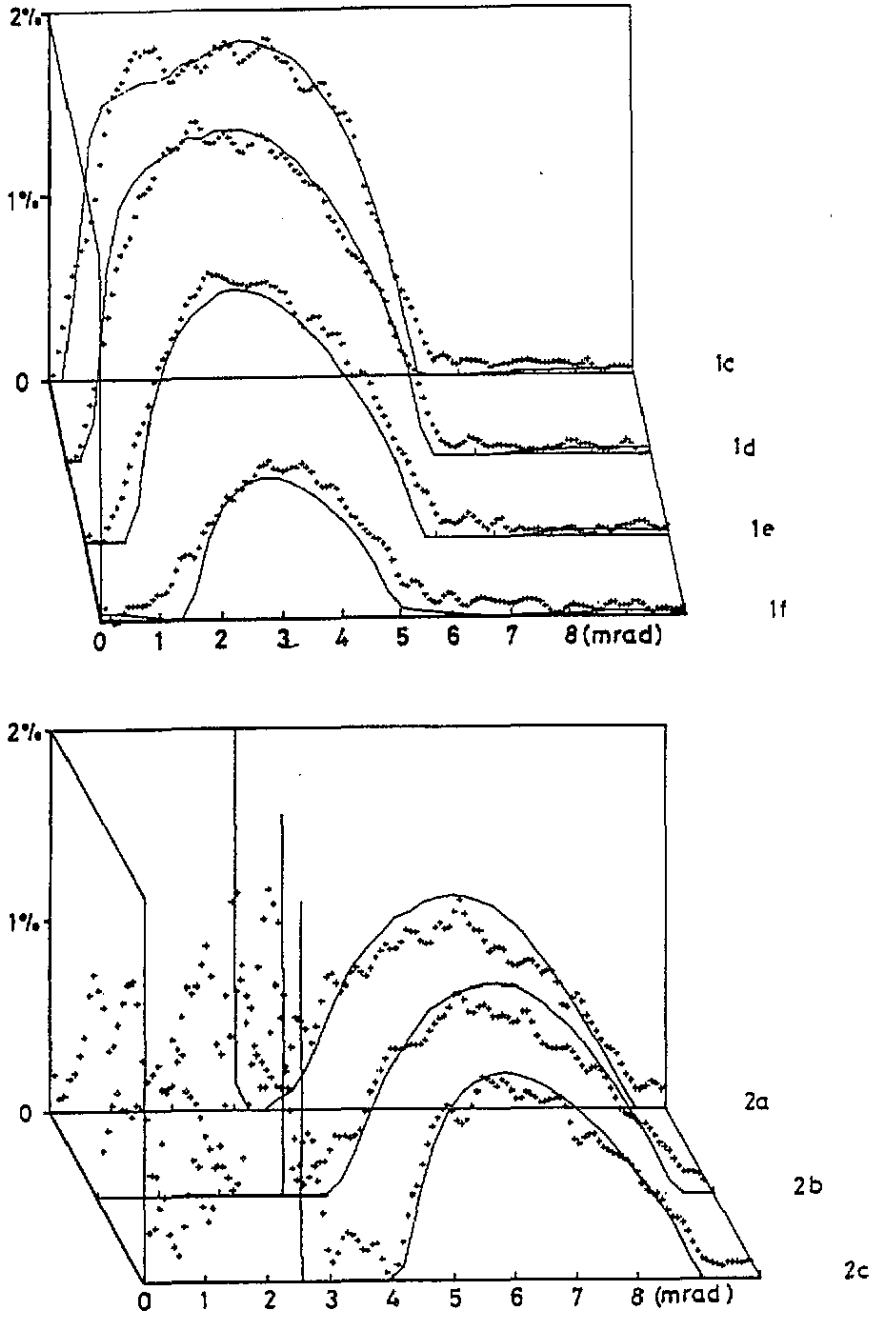


**Figure 6.** As in figure 4. K at 4 K; LMTO calculation.

was also reached by Sormann and Šob [39] who used different potentials and the augmented plane wave method and compared their calculations with the experimental results presented

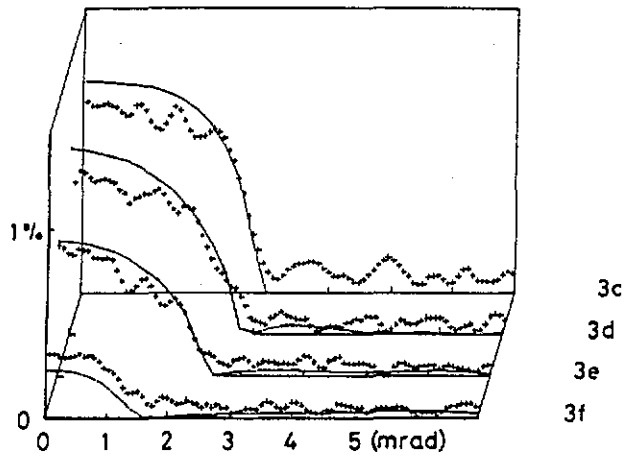


**Figure 6.** (Continued)

in this paper.

Since these several independent particle calculations yield good agreement with observed HMCs, we conclude that the general effect of electron–positron correlations must be the same in the higher zones as it is in the first zone.

In contrast, very little can be said about the momentum dependence of the enhancement in the higher zones. A constant enhancement independent of momentum might be compatible with the data while a very strong momentum dependence would probably not fit the observations. A careful analysis of the data in the first zone to obtain the momentum dependence of enhancement has not been done, but we note that a preliminary analysis [18] seems to imply an enhancement function in agreement with the results of Hyodo *et al* [8]. They found that the early work of Kahana and Carbotte [9–11] fits the data better than more recent calculations. If it could be shown that the many body effects of creating the polarization cloud around the positron did not alter the higher momentum components of the wave functions, or altered them in a known manner, then the shapes and intensity of these components would become a sensitive test of the lattice potential models for single-particle descriptions of electrons in these simple metals.

An additional test of the independent particle model calculations was made by performing KKR band calculations and subsequent momentum density determinations. The KKR band calculations are quite different from the LMTO calculations in that they were not self-consistent and did not include f states [7]. The subsequent analysis of the HMCs was made exactly as for the LMTO results. Despite the differences between the two methods, the resulting HMCs are quite similar. The KKR result also agrees well with experiment, although the amplitudes are slightly smaller than the LMTO calculation. This difference may be due to the fact that the f-states are missing in the KKR basis set. As shown below, the f-contribution is small, but its relative importance increases in the HMC. The KKR–LMTO comparison confirms that the IPM calculations describe the HMCs well, which indicates that the important positron-electron correlation effects do not disturb the IPM results much in this simple one-electron metal.

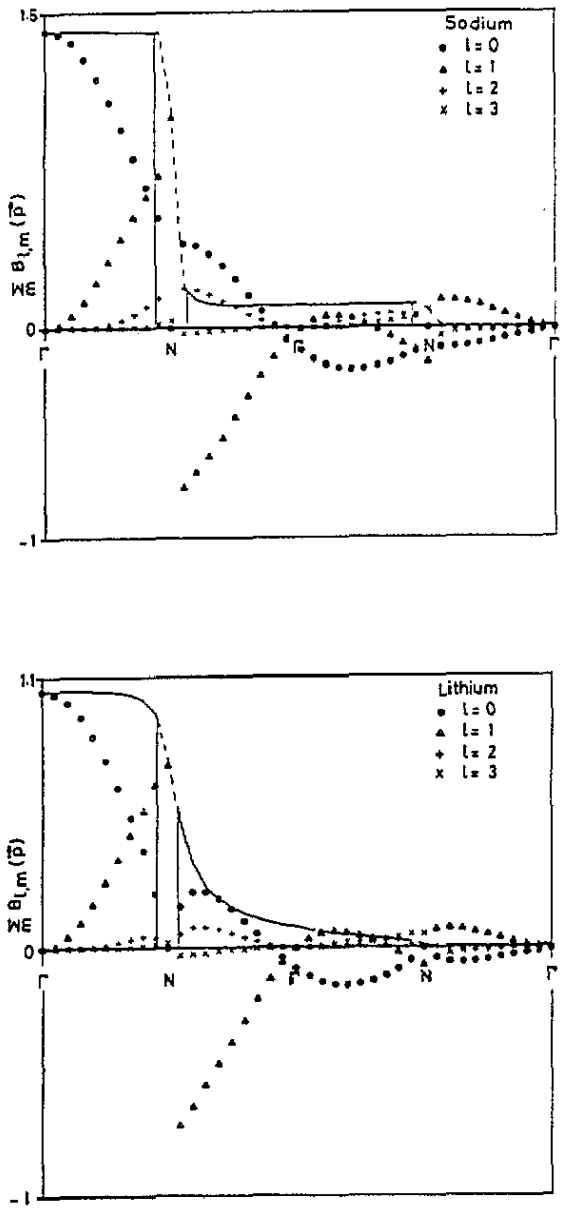


**Figure 7.** Angular momentum decomposition of the momentum amplitude $\sum_m B_{lm}(\boldsymbol{p})$ (see equation (11)) along the [110] direction in Li, Na, and K.

Despite the similarities in the occupied bands in Li, Na, and K, the higher-momentum components of Li are strikingly different in shape from those in Na and K. The reason for this can be understood from an angular decomposition of the momentum distributions. Figure 7 shows the quantities $\sum_m B_{lm}(\boldsymbol{p})$, which upon summation with respect to $l$ and

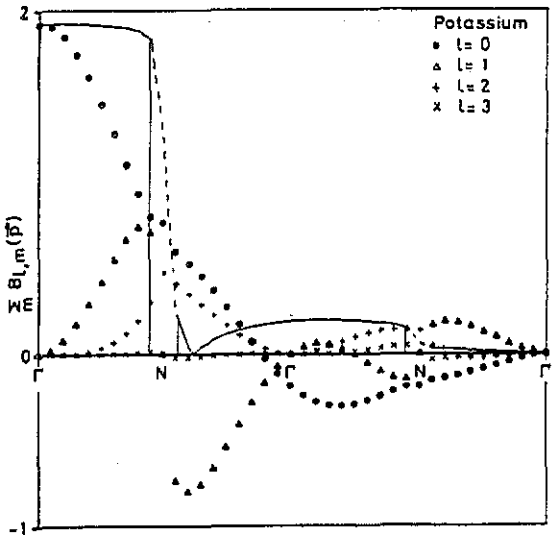


**Figure 7.** (Continued)

squaring yield $\rho(p)$ along the [110] direction. Symmetry plays an important role but the detailed behaviour of the wave functions cannot be overlooked. In Li and Na the lowest level at N (the centre of the nearest zone face) is a pure p level.† Hence at N the s and d terms are zero by symmetry and only the p term is present. Owing to its odd parity this term is discontinuous at N. Away from N the s and d terms increase again and in the second Brillouin zone they begin to interfere destructively with the large p term. In Li this gives rise to the particular shape of the HMC in that zone.‡ The case of Na is very similar except that the s and d terms are larger than in Li. They are therefore more successful in the destructive interference with the p term, making the sum over all $l$ inside the Fermi surface in the second zone nearly independent of momentum. In K however the situation is quite different. The s and d like states at N have now become the lowest level due to the presence of the $3d$ band not far above the Fermi level. Thus at the N point the s and d terms may be large while the p term must pass through zero. The interference between the s, p, and d terms now results in a zero in their sum somewhere between N and $\Gamma'$ and thus a minimum in the momentum density. This minimum occurs over a surface that crosses the [110] axis near $(0.62, 0.62, 0)(2\pi/a)$ and is reminiscent of the so called Cooper minimum in photoemission spectroscopy [40, 41]. This minimum in the momentum density is not directly visible in the data because of the integration over one dimension.

† On the basis of the pseudopotential arguments of Cohen and Heine [49] and Heine and Weaire [50] (see also [51]) one would expect the lowest level to be p like for all alkali metals. Note that the reciprocal lattice vectors are at $q/2k_F = 1.14$ for monovalent BCC elements, while the pseudopotential becomes positive at $q/2k_F = 0.8$–$0.9$ and hence $V_{110} > 0$, making the lowest level at N a p bonding state. However, in the progression from Li to Na to K, the d band moves down to a position just above the Fermi level. In doing so the d-like $N_1$ level is pushed down by hybridization. Somewhere near Na the $N_1$ level passes through the $N_{1'}$ level and becomes the lowest one.

‡ A Hartree–Fock calculation of the electron momentum density in Li by Dovesi *et al* [52]) has yielded comparable results.

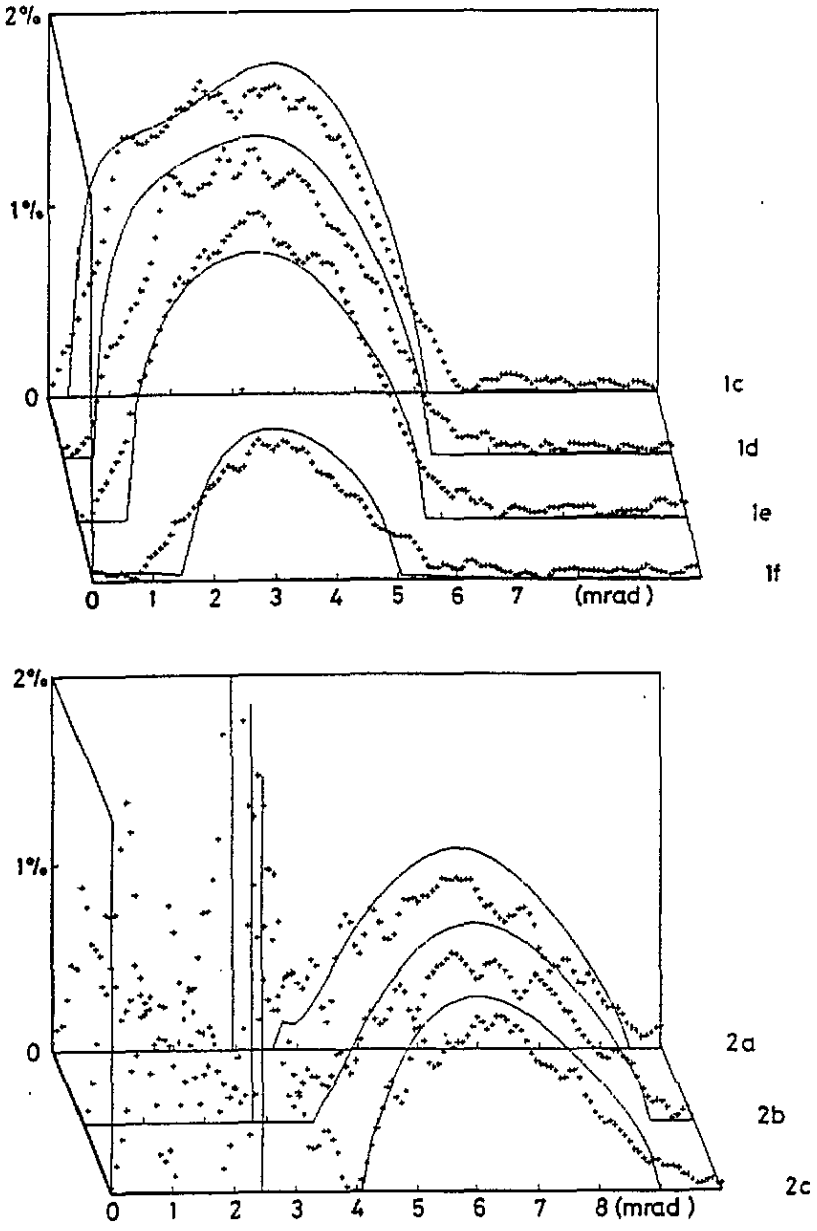


**Figure 8.** As in figure 4. Potassium at 75 K; LMTO calculation.

In the above discussion the small f-terms have been ignored. Figure 7 however shows that their importance grows at high momentum. As mentioned, this f-contribution may be one reason why the KKR and LMTO calculations are slightly different. In all three metals the f component is important near the N point and whenever the s, p, and d terms cancel.

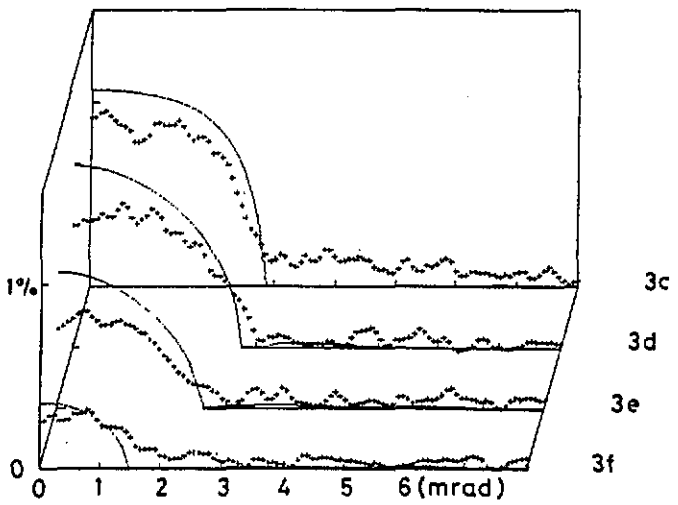


**Figure 8.** (Continued)

*5.2. Thermal effects on momentum distributions*

In this section we discuss K because it has been measured at various temperatures with both the long slit [8] and the two-dimensional geometry of the present work.

We describe first the calculations we have performed to evaluate the temperature effects. Then we discuss the two dimensional measurements for potassium at 4 K and 75 K, and long-slit data at these and higher temperatures.

We have performed two self-consistent band structure calculations for K using a lattice dimension of 9.882 au for $T = 4.2$ K, and 9.916 au for $T = 91$ K. The momentum distributions obtained are very similar. We note an overall increase of 1% in the second calculation, reflecting the contraction of the reciprocal lattice with temperature. The increase is about 1% everywhere except for the [110] zone, which remained nearly constant. This non-uniform variation shows that the wave functions are a function of the lattice spacing.

We show in figure 8 the comparison between the calculation for $a = 9.916$ au, using equation (16) for the Debye–Waller effect, and the experimental data measured at 75 K. Comparison of figures 8 and 6 shows the expected decrease in intensity as the temperature is raised, both in the calculation and in the experimental data. A measurement of the integrated intensity of the HMC at 4.2 K and 75 K yields a ratio of $0.89 \pm 0.04$ , in fair agreement with values calculated from equations (15) and (16) of 0.95 and 0.93, respectively. While somewhat better agreement with intensities is achieved, our data are not precise enough to distinguish the small change in shape of the HMC's expected when using equation (16) instead of equation (15) chiefly because of uncertainties in the core subtraction process.

We have also compared our calculations of the Debye–Waller factor with the long-slit data of Hyodo *et al* [8] at 91 K, 199 K, and 298 K. Their data show a decrease in intensity of the higher momentum components as temperature rises, similar to and slightly larger than that calculated from our equation (16).

It will be important in the future to go beyond the underlying assumption of the same value of $W$ for all electrons. A more general treatment is necessary, one which separates

the motion of electrons (and the positron) based on their binding to the nuclei along the lines of [42].

Our analysis shows that thermal effects are large and may even influence data at low temperature when the ionic masses are small, and their zero-point motion is large.

### *5.3. Other deductions from data*

*5.3.1. Fermi surface of Li.* These data have been analysed to determine the anisotropy of the Fermi surface. As expected, the radius was larger in the (110) directions than in other directions, the maximum difference being $2.8 \pm 0.6\%$ [35]. This is in general agreement with calculations using a non-local energy-dependent mass operator in the context of the density functional formalism [43]. (Another experiment by positron annihilation has been analysed to give $3.5 \pm 0.3\%$ [44].)

*5.3.2. Charge density waves in K.* [45]. The existence of charge density waves may be seen if such waves are aligned and lie in the preferred [110] direction [46]. In this situation a bulge of about 6% should be expected [47] whereas our observations show sphericity to 0.6%. If 20% of the charge density waves were aligned and the remainder random, they might still be observed as an additional smearing of the Fermi surface. The observed smearing is compatible with the experimental resolution. No extra smearing due to a possible charge density wave is detectable.

## 6. Conclusions

This paper has presented accurate measurements of the two dimensional projection of the momentum distribution of photons from positrons annihilating in the alkali metals Li, Na, and K. The data exhibit interesting structure especially in the HMCs of the electron–positron wave function. Although the band structure and momentum density in the first zone are very similar in the three alkali metals studied, there are important differences between these metals in the higher zones. Calculations of the momentum density in these higher zones, employing the independent particle model and based on local density electron band structures, are in excellent general agreement with experimental results. The comparisons show that this experimental method is more sensitive to details of the lattice potential than any other technique.

The momentum distributions also show changes as the temperature is varied. We suggest that both the magnitude and temperature dependence of this effect are different for valence and core electrons, and that a deeper analysis of the Debye–Waller effect is needed.

In conclusion, the positron annihilation technique is shown to be useful to test details of lattice potentials for electrons and positrons, to examine some of the many-body electron gas effects, and to probe thermal effects on the motion of electrons. Finally, these data are also the best illustrations available of the Bloch structure of wave functions in a periodic lattice.

## Acknowledgments

We are indebted to our many colleagues with whom we have discussed these results, and to partial support by the Swiss National Science Foundation, by the North Atlantic Treaty Organization, the Japan Society for the Promotion of Science, and the Interfaculty Reactor Institute of the Delft University of Technology.

## References


[1] For a review see the articles by Berko S and Mijnarends P E 1983 *Positron Solid State Physics* ed W Brandt and A Dupasquier (Amsterdam: North-Holland), and the series of conference proceedings called *Positron Annihilation*: Kajcsos Z and Szeles C (ed) 1991 *Mater. Sci. Forum* **105–110**; Dorikens-Vanpraet L, Dorikens M and Segers D (ed) 1988 (Singapore: World Scientific); Jain P C, Singru R M and Gopinathan K P (ed) 1985 (Singapore: World Scientific); Coleman P G, Sharma S C and Diana L M (ed) 1982 (Amsterdam: North-Holland); Hasiguti R R and Fujiwara K (ed) 1979 (Sendai: Japan Institute of Metals); Trumpy G (ed) 1976 Abstracts only; 1973 papers published individually in *Appl. Phys.*; McKee B T A and Stewart A T (ed) 1971 Abstracts only; Stewart A T and Roellig L O (ed) 1967 (New York: Academic)

[2] DeBenedetti S, Cowan C E, Konneker W R and Primakoff H 1950 *Phys. Rev.* **77** 205

[3] Ferrell R A 1956 *Rev. Mod. Phys.* **28** 308

[4] Donaghy J J and Stewart A T 1967 *Phys. Rev.* **164** 396

[5] Kim S M and Stewart A T 1975 *Phys. Rev.* B **11** 2490

[6] Singh A K, Manuel A A, Jarlborg T, Mathys Y, Walker E and Peter M 1986 *Helv. Phys. Acta* **59** 410

[7] Oberli L, Manuel A A, Sachot R, Descouts P, Peter M, Rabou L P L M, Mijnarends P E, Hyodo T and Stewart A T 1985 *Phys. Rev.* B **31** 1147

[8] Hyodo T, McMullen T and Stewart A T 1986 *Phys. Rev.* B **33** 3050

[9] Kahana S 1960 *Phys. Rev.* **117** 123

[10] Kahana S 1963 *Phys. Rev.* **129** 1622

[11] Carbotte J P and Kahana S 1965 *Phys. Rev.* **139** A213

[12] Hede B B J and Carbotte J P 1972 *J. Phys. Chem. Solids* **33** 727

[13] Fujiwara K, Hyodo T and Ohyama J 1972 *J. Phys. Soc. Japan* **33** 1047

[14] Fujiwara K and Hyodo T 1973 *J. Phys. Soc. Japan* **35** 1664

[15] Sormann H and Puff W 1985 *Positron Annihilation* ed P C Jain, R M Singru and K P Gopinathan (Singapore: World Scientific) pp 161–3

[16] Mader J, Berko S, Krakauer H and Bansil A 1976 *Phys. Rev. Lett.* **37** 1232

[17] Mijnarends P E and Singru R M 1979 *Phys. Rev.* B **19** 6038

[18] Oberli L, Manuel A A, Singh A K, Jarlborg T, Rabou L P L M, Mijnarends P E, Hyodo T and Stewart A T 1985 *Positron Annihilation* ed P C Jain, R M Singru and K P Gopinathan (Singapore: World Scientific) pp 251–3

[19] Krogh Andersen O 1975 *Phys. Rev.* B **12** 3060

[20] Jarlborg T and Arbman G 1977 *J. Phys. F: Met. Phys.* **7** 1635

[21] Skriver H L 1984 *The LMTO method* (Berlin: Springer)

[22] Singh A K and Jarlborg T 1985 *J. Phys. F: Met. Phys.* **15** 727

[23] Arponen J and Pajanne E 1985 *Positron Annihilation* ed P C Jain, R M Singru and K P Gopinathan (Singapore: World Scientific) pp 21–33

[24] Rubaszek A, Stachowiak H, Boronski E and Szotek Z 1984 *Phys. Rev.* B **30** 2490

[25] Rubaszek A and Stachowiak H 1985 *J. Phys. F: Met. Phys.* **15** L231

[26] Boronski E and Nieminen R M 1986 *Phys. Rev.* B **34** 3820

[27] Jarlborg T and Singh A K 1987 *Phys. Rev.* B **36** 4660

[28] Barbiellini B, Genoud P and Jarlborg T 1991 *J. Phys.: Condens. Matter* **3** 7631

[29] Nieminen R M and Manninen M J 1979 *Positrons in Solids* ed P Hautojärvi (Berlin: Springer) pp 145–95

[30] Brandt W, Eder L and Lundqvist S 1966 *Phys. Rev.* **142** 165

[31] Hosemann R and Bagchi S N 1962 *Direct Analysis of Diffraction by Matter* (Amsterdam: North-Holland) p 275

[32] Mijnarends P E and Bansil A 1990 *J. Phys.: Condens. Matter* **2** 911

[33] Bisson P E, Descouts P, Dupanloup A, Manuel A A, Perreard E, Peter M and Sachot R 1982 *Helv. Phys. Acta* **55** 100

[34] Oberli L 1985 *PhD Thesis* Université de Genève

[35] Oberli L, Manuel A A, Sachot R, Descouts P and Peter M 1985 *Phys. Rev.* B **31** 6104

[36] Fujiwara K 1982 *Positron Annihilation* ed P G Coleman, S C Sharma and L M Diana (Amsterdam: North Holland) pp 615–24

[37] Stewart A T, Brisco C V and Steinberger J S 1990 *Can. J. Phys.* **68** 1362

[38] Shoenberg D 1969 *The Physics of Metals. 1. Electrons* ed J M Ziman (Cambridge: Cambridge University Press) pp 62–112

[39] Sormann H and Šob M 1990 *Phys. Rev.* B **41** 10529

[40] Cooper J W 1964 *Phys. Rev. Lett.* **13** 762

[41] Wehner P S, Stöhr J, Apai G, McFeely F R, Williams R S and Shirley D A 1976 *Phys. Rev.* B **14** 2411

[42] Stott M J and West R N 1978 *J. Phys. F: Met. Phys.* **8** 635
[43] MacDonald A H 1980 *J. Phys. F: Met. Phys.* **10** 1737
[44] Triftshäuser W, Eckert A, Kögel G and Sperr P 1992 *Mater. Sci. Forum* **105–110** 501
[45] Overhauser A W 1978 *Adv. Phys.* **27** 343
[46] Overhauser A W 1974 *Phys. Rev.* B **3** 3173
[47] Sharma S M and Gupta S C 1983 *J. Phys. F: Met. Phys.* **13** L7
[48] After Mijnarends P E 1979 *Positrons in Solids* ed P Hautojärvi (Berlin: Springer) pp 25–88.
The entries for the Debye–Waller factor for K at 78 K in table 2.3 of this reference are in error and should be replaced by the corresponding values given in table 2 of this paper.
[49] Cohen M L and Heine V 1970 *Solid State Physics* vol 24, ed H Ehrenreich, F Seitz and D Turnbull (New York: Academic) p 37
[50] Heine V and Weaire D 1970 *Solid State Physics* vol 24, ed H Ehrenreich, F Seitz and D Turnbull (New York: Academic) p 249
[51] Hafner J and Heine V 1983 *J. Phys. F: Met. Phys.* **13** 2479
[52] Dovesi R, Ferrero E, Pisani C and Reotti C 1983 *Z. Phys.* B **51** 195